MOLECULAR PHYSICS, 1997, VOL. 92, NO. 2, 187–195

# Multiphase equilibria using the Gibbs ensemble Monte Carlo method

By J. N. CANONGIA LOPES
Centro de Química Estrutural, Instituto Superior Técnico, 1096 Lisboa, Portugal

and D. J. TILDESLEY
Department of Chemistry, Imperial College, London SW7 2AZ, UK

(*Received 20 January 1997; revised version accepted 2 April 1997*)

The Gibbs ensemble simulation method is extended to multiphase equilibria by increasing the number of boxes that can be used concurrently in the simulation. Atoms are moved within each box and pairs of boxes are selected at random for the volume and particle exchange moves. The equivalence between the Gibbs ensemble with an arbitrary number of boxes and the corresponding canonical ensemble is established. Simulations of two-component, three-phase equilibria and three-component, four-phase and three-phase equilibria are demonstrated for simple model systems, and the model phase diagrams are determined.

## 1. Introduction

Since its introduction some years ago [1], the Gibbs ensemble Monte Carlo, technique has proved to be one of the most effective ways of directly simulating two coexisting phases in equilibrium, and it is being applied successfully to the study of liquid–vapour, osmotic and liquid–liquid equilibria in a wide range of fluids and fluid mixtures [2].

In the Gibbs method two bulk phases are simulated as two separate subsystems, avoiding the problems with the direct simulation of the interface between the two homogeneous phases. Equilibrium is attained by allowing the subsystems to undergo three types of move: random particle movements within each subsystem; complementary expansion/contraction of the subsystems; and a transfer of one particle from one subsystem to the other. The first type of move is responsible for the internal equilibrium within each subsystem, and the latter two moves ensure the equality of pressure and chemical potential between the phases.

In the present work the Gibbs ensemble method has been extended to the study of more than two coexisting phases by increasing the number of subsystems involved in the simulation. In the following section the problems associated with such an extension, i.e., the soundness of such an extended ensemble and the way to sample it using a Monte Carlo method will be dealt with in more detail, and later some examples of systems showing multiple phase separation will be presented.

An understanding of fluid systems is associated strongly with the determination of their phase diagrams. The phase rule indicates that in the case of multi-component systems these diagrams can be quite complicated, due to the presence of zones dominated by multiple phase coexistence. The Gibbs ensemble Monte Carlo technique can be used in the form presented in this paper to simulate these phase diagrams directly.

## 2. Theory

The theoretical basis of the Gibbs ensemble Monte Carlo method has been reviewed by Panagiotopoulos [2] and Smit [3]. Smit showed formally that the free energy density of the Gibbs ensemble is identical to the free energy density of the canonical ensemble in the thermodynamic limit, i.e., the ensembles can be regarded as equivalent.

The partition function of the Gibbs ensemble can be written as a combination of the partition functions of each system. In the case of two subsystems:

$$\bar{Q}_{NVT} = \sum_{n_1=0}^{N} \int_0^V \mathrm{d}V_1 Q_{n_1 V_1 T} Q_{n_2 V_2 T}, \qquad (1)$$

where $N$, $V$ and $T$ are the total number of particles, the volume and the temperature of the system, $n_1$ is the number of particles in box 1 and $V_1$ denotes the volume of the first box. $\bar{Q}$ and $Q$ represent the Gibbs ensemble and canonical ensemble partition functions

(the partition functions of each subsystem for a given $n_1$ and $V_1$ correspond to canonical ensembles). The free energy density of the Gibbs ensemble, $\bar{f}(\rho)$ is defined as

$$\bar{f}(\rho) = \lim_{\substack{V\to\infty \\ N/V=\rho}} \left[ -\frac{1}{\beta V} \ln \bar{Q}_{NVT} \right], \tag{2}$$

and is identical to the free energy density of the corresponding canonical ensemble [3]. Furthermore, it has been shown [3] that in the case of a single phase (high temperature) both boxes in the Gibbs ensemble will have the same density, whereas in the case of a system exhibiting a first-order phase transition each box will represent one of the two coexisting phases.

In the case of $s$ subsystems (with $V = \sum_{i=1}^{s} V_i$ and $N = \sum_{i=1}^{s} N_i$), the corresponding partition function can be written using a recursive argument: first we write the Gibbs ensemble partition function of two subsystems (the last two) with a total number of particles just $N_2 = n_s + n_{s-1}$ and a total volume $V_2 = V_s + V_{s-1}$. These two subsystems are equivalent to one $(N_2, V_2, T)$ canonical ensemble.

$$\bar{Q}_2 = \sum_{n_{s-1}=0}^{N_2} \int_0^{V_2} \mathrm{d}V_{s-1} Q_{n_{s-1}V_{s-1}T} Q_{n_s V_s T_s}. \tag{3}$$

Now a third subsystem can be added (the total number of particles becoming $N_3 = n_s + n_{s-1} + n_{s-2}$) and a new Gibbs ensemble partition function (again similar to equation (1)) can be written using the previous partition function as a whole:

$$\begin{aligned} \bar{Q}_3 &= \sum_{n_{s-2}=0}^{N_3} \int_0^{V_3} \mathrm{d}V_{s-2} Q_{n_{s-2}V_{s-2}T} \bar{Q}_2 \\ &= \sum_{n_{s-2}=0}^{N_3} \sum_{n_{s-2}=0}^{N_2} \int_0^{V_3} \mathrm{d}V_{s-2} \\ &\quad \times \int_0^{V_2} \mathrm{d}V_{s-1} Q_{n_{s-2}V_{s-2}T} Q_{n_{s-1}V_{s-1}T} Q_{n_s V_s T}. \end{aligned} \tag{4}$$

The procedure can be repeated until all the subsystems are added. The final expression takes the form

$$\begin{aligned} \bar{Q}_s &= \sum_{n_1=0}^{N} \sum_{n_2=0}^{N-n_1} \cdots \sum_{n_{s-1}=0}^{N-(n_1+\cdots+n_{s-2})} \int_0^{V} \mathrm{d}V_1 \\ &\quad \times \int_0^{V-V_1} \mathrm{d}V_2 \cdots \int_0^{V-(V_1+\cdots+V_{s-2})} \mathrm{d}V_{s-1} \prod_{i=1}^{s} Q_{n_i V_i T} \end{aligned} \tag{5}$$

or, substituting the expressions for each canonical ensemble

$$\begin{aligned} \bar{Q}_s &= \frac{1}{\Lambda^{3N} V^{s-1} N!} \sum_{n_1=0}^{N} \sum_{n_2=0}^{N-n_1} \cdots \sum_{N_{s-1}=0}^{N-(n_1+\cdots+n_{s-2})} \binom{N}{n_1} \\ &\quad \times \binom{N-n_1}{n_2} \cdots \binom{N-(n_1+\cdots+N_{s-2})}{n_{s-1}} \\ &\quad \times \int_0^{V} \mathrm{d}V_1 \int_0^{V-V_1} \mathrm{d}V_2 \cdots \int_0^{V-(V_1+\cdots+V_{s-2})} \mathrm{d}V_{s-1} \\ &\quad \times \prod_{i=1}^{s} V_i^{n_i} \int \mathrm{d}\xi_i^{n_i} \exp\left(-\beta U_i(n_i)\right). \end{aligned} \tag{6}$$

In all steps the equivalence between a Gibbs ensemble and a corresponding canonical ensemble is clear. This equivalence is as true for the many-box Gibbs ensemble as for the original two-box ensemble. The number of degrees of freedom of the extended Gibbs ensemble is larger than in the original method: the minimum free energy surface is no longer bidimensional but a $2(s-1)$-dimensional hypersurface. In a system exhibiting a first-order phase transition, each box will converge to one of the equilibrium densities. As we lose phases by changing conditions some of the boxes will exhibit identical densities. In the case of more than 2 phases at least 3 boxes will have different densities. As previously shown [3], the driving force for the equilibration in the Gibbs ensemble is the minimization of the surface free energy, causing the system to split into one homogeneous phase in each box.

The statistical weight of a given configuration with $n_1, n_2, \ldots, n_s$ particles in the 1st, 2nd, $\ldots$, $s$th subsystem of $V_1, V_2, \ldots, V_s$ volume is (cf. equation (6))

$$\begin{aligned} p(n_1, n_2, \ldots, n_s; V_1, V_2, \ldots, V_s; T) &\propto \frac{V_1^{n_1} V_2^{n_2} \ldots V_s^{n_s}}{n_1! n_2! \ldots n_s!} \\ &\quad \times \exp\left( -\beta \sum_{i=1}^{s} U_i(n_i) \right). \end{aligned} \tag{7}$$

Since all the Monte Carlo moves performed during a Gibbs ensemble Monte Carlo simulation are either inside each simulation box (a particle displacement) or between a pair of boxes (volume and particle exchanges), the acceptance criteria for producing a Markov chain of configurations with a probability distribution equivalent to equation (7) are the same whether the system has two or more simulation boxes. For volume and particle exchange, two boxes are selected at random and only their respective volume, total potential energy and number of particles need to be considered. These rules have been reported elsewhere [4].

We will demonstrate that the Gibbs method can be extended in this way by considering a number of simple examples.

## 3. Three-phase boundaries in binary mixtures

### 3.1. *Computational aspects*

All the simulations presented in this paper were produced using mixtures of Lennard–Jones atoms studied using constant volume Gibbs ensemble Monte Carlo simulations. All simulations were started from a face-centred cubic lattice configuration with species placed randomly on the lattice. Except where otherwise stated, the initial volume, density and composition of each box were identical. Binary mixtures exhibiting liquid–liquid–vapour (LLV) and liquid–vapour (LV) equilibria were simulated using three simulation boxes. In cases where only two phases were present (LV or liquid–liquid (LL) equilibria), additional two-box simulations also were performed to check the results.

In order to fulfil the conditions of microscopic reversibility at every step of the simulation the type of Monte Carlo move to be performed is selected at random with a predetermined probability. After the selection of the type of move, the box or pair of boxes to be affected by the move also is selected at random. Finally, in the particle displacement or interchange moves, one particle from one of the selected boxes also is picked randomly. The microscopic reversibility of such an algorithm has been demonstrated by Rull *et al.* [5]. Their acceptance criteria (closely related to the original criteria proposed by Panagiotopoulos *et al.* [4]) have been followed.

The pre-fixed ratio for each type of move was chosen by considering the efficiency with which the simulation attains equilibrium. The number of possible different moves between boxes during particle and volume exchanges is given by $s(s-1)/2$. Since it is important that equilibrium is established between all boxes, the number of exchange moves has to increase accordingly.

The displacement moves were performed by adding a random value from a uniform distribution to the co-ordinates of the particle undergoing the displacement. The maximum value of the displacement in each box was updated in order that the acceptance ratio of the moves stayed at 50%. The volume exchanges also were chosen randomly from a uniform distribution, and the maximum volume exchange was adjusted to produce an acceptance ratio of 50% for any given pair of boxes. During this type of move the potential energy in each of the boxes affected by the change was calculated using the scaling properties of the Lennard-Jones potential (separation of the repulsive and attractive terms). The particle exchange moves were performed in two complementary ways selected with fixed probability: either one particle is moved from one box to another (0·9 probability) or two particles of different species (and different boxes) are swapped (0·1 probability).

Two aspects of the method became evident during the multi-box simulations. First, whenever the number of phases is smaller than the number of boxes, the extra degree(s) of freedom allow the size and number of particles of each box to sample several points in the minimum energy hypersurface. This means that one or several of the boxes can 'contract' in terms of $N$ and $V$ until it vanishes or until finite-size effects become dominant. This type of problem has been noted already for two-box simulations in one-phase systems. Second, it was found that it is much easier to equilibrate two dense fluids (liquids) when they are in equilibrium with their vapour (the LLV situation). The composition within each liquid reaches its equilibrium value since both are in equilibrium with the vapour, and the rate of acceptance for particle exchange moves between liquid and vapour is much higher than between two liquids. Particle interchange from one liquid to the other occurs through the vapour phase.

In figure 1 two control plots for the simulation of mixture I are shown (see table 2 later). The plots show the first 5000 cycles, where the density and composition equilibration processes in each box are easily recognizable. In a typical simulation some 450–600 particles were used to generate 40–80 thousand simulation cycles (in each cycle a number of displacement moves equal to the total number of particles plus a number of volume and particle exchange moves given by the predetermined ratios are attempted). Equilibration periods

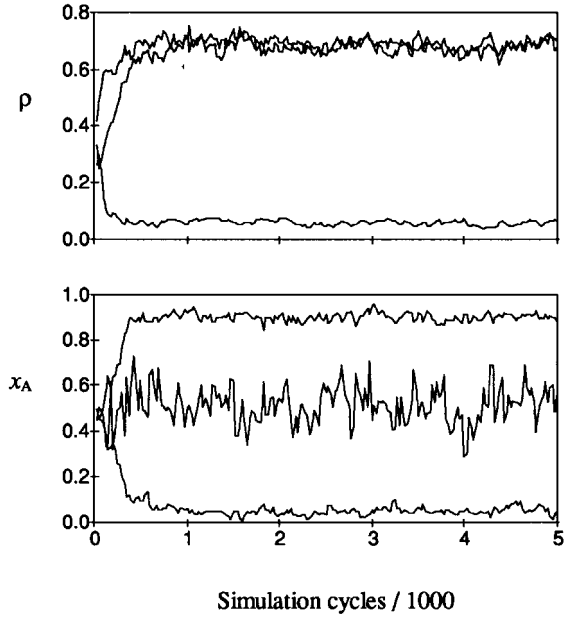


Figure 1. Reduced density $\rho$ and mole fraction $x_A$ of component A, in the three-phase region (LLV) of mixture I (equimolar composition, cf. table 1) as a function of the number of cycles generated in a three-box Gibbs ensemble simulation.

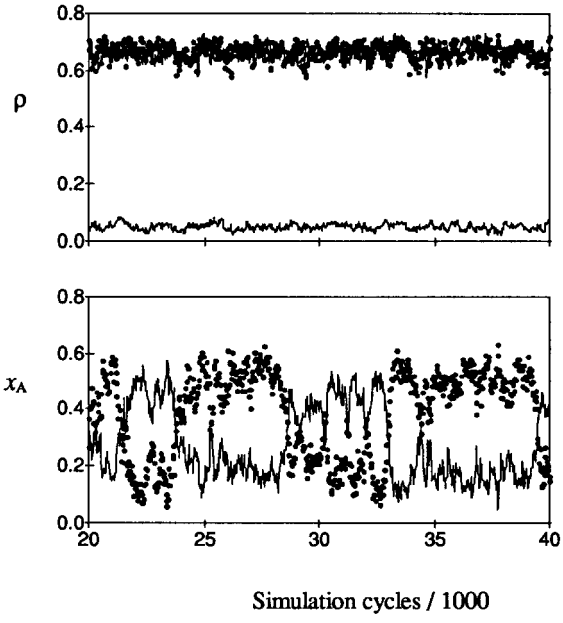


Figure 2. Reduced density $\rho$ and mole fraction $x_A$ of component A, in the three-phase region (LLV) of mixture IV (0·335 mole fraction in A and B, cf. table 2) as a function of the number of cycles generated in a three-box Gibbs ensemble simulation. The composition plot shows only the two liquid phases (plotted using a solid curve and dots). The system exhibits identity swapping between the two simulation boxes containing the liquid phases.

ranged from 10 to 40 thousand steps, depending on the number and relative density of the phases present.

In figure 2 two similar control plots for the simulation of mixture V are shown. In this case the data presented corresponds to simulation cycles performed after equilibration of the system (LLV equilibria) and shows the occurrence of an identity change between the two boxes containing the two immiscible liquids. This finite-size effect starts to be relevant when the composition of the system approaches values close to the end of the immiscibility window (LLV to LV phase transition).

### 3.2. *Simulation results*

Two types of binary mixture were considered (see table 1). In mixture I both components have the same size and volatility: indeed they are identical Lennard-Jones particles. The liquid–liquid immiscibility occurs because of the low value attributed to the cross-interaction Lennard-Jones parameter $\varepsilon_{AB}$. In mixture II the components have quite different volatility, and in this case liquid–liquid separation occurs because the less volatile component excludes the other from its presence.

A mixture similar to I was studied previously by Panagiotopoulos *et al.* [4]. In their case, since both the value of $\varepsilon_{AB}$ and the reduced temperature were higher

Table 1. Interaction parameters and reduced temperature for the mixtures studied. The Lennard-Jones diameter is the same for all interactions, $\sigma = 1$.

| Mixture | $\varepsilon_{AA}$ | $\varepsilon_{BB}$ | $\varepsilon_{CC}$ | $\varepsilon_{AB}$ | $\varepsilon_{AC}$ | $\varepsilon_{BC}$ | $T$ |
|---|---|---|---|---|---|---|---|
| I | 1 | 1 | — | 0·7 | — | — | 1·0 |
| II | 0·7 | 1·4 | — | 0·89 | — | — | 0·8 |
| III | 1 | 1 | 1 | 0·7 | 0·7 | 0·7 | 1·0 |
| IV | 1 | 1 | 1 | 0·6 | 0·6 | 0·6 | 1·0 |
| V | 1 | 1 | 1 | 0·6 | 1 | 1 | 1·0 |

(0·75 and 1·15, respectively), liquid–liquid immiscibility did not occur, the mixture exhibiting an azeotrope. Making this mixture slightly less ideal and/or lowering the temperature leads to the liquid–liquid immiscibility. This was observed by van Leeuwen *et al.* [6] for mixtures with pure-component LJ parameters corresponding to argon and krypton using a variable cross-interaction parameter. However, the three-phase line could not be determined exactly by extrapolation, due to the large pressure fluctuations on the LL two-phase side.

Table 2 presents the results for thermodynamic properties on the coexistence curves (LL, LV and LLV equilibria) of the two mixtures. These results were tested for their internal consistency by considering (i) the pressure values in the three simulation boxes, (ii) the agreement of results in the two-phase region (LL or LV) considering two or three box simulations, and (iii) the calculation of the chemical potential in the three boxes for selected points in the diagrams. The data corresponding to the two pure components also were checked against the data reported by Panagiotopoulos [1] and Adams [7].

The *p-x-y* phase diagrams for each mixture are shown in figures 3 and 4. The phase diagram shown in figure 3 is probably one of the most common whenever two liquids of similar volatility are only partially miscible. Mixtures of normal alkanes with their perfluoro counterparts (e.g., methane + tetrafluoromethane or cyclohexane + perfluorocyclohexane) are typical examples of such systems [8]. The phase diagram presented in figure 4 is typical of systems where the two pure components have very different volatility (e.g. n-pentane+ nitrobenzene).

## 4. Ternary mixtures

### 4.1. *Computational aspects*

In the ternary system exhibiting triple liquid immiscibility (mixture IV) four simulation boxes were used when the system split into four phases in equilibrium (three liquid and one vapour phase, LLLV). Otherwise three boxes were used to simulate LLV equilibria. The

Table 2. Results for phase coexistence properties of binary mixtures: $p$–$x$–$y$ and density data. The numbers in parentheses indicate the uncertainty in the last decimal digits, i.e., 0·026(5) means 0·026 ± 0·005. These errors are one standard deviation in the block averages and are calculated through the production phase.

| $x_{A\,total}$ | $p_{vap.}$ | $x_{A\,liq.1}$ | $x_{A\,liq.2}$ | $y_A$ | $\rho_{liq.1}$ | $\rho_{liq.2}$ | $\rho_{vap.1}$ |
|---|---|---|---|---|---|---|---|
| | | | Mixture I | | | | |
| 0·00 | 0·026(5) | 0·000 | 0·000 | 0·000 | 0·705(19) | 0·706(18) | 0·031(6) |
| 0·04 | 0·036(6) | 0·020(8) | 0·024(8) | 0·242(60) | 0·701(20) | 0·701(20) | 0·044(6) |
| 0·10 | 0·043(60 | 0·059(20) | 0·063(19) | 0·416(87) | 0·684(22) | 0·689(23) | 0·055(8) |
| 0·20 | 0·051(6) | 0·153(24) | 0·142(23) | 0·517(90) | 0·662(21) | 0·660(20) | 0·069(8) |
| 0·50 | 0·052(7) | 0·868(29) | 0·114(32) | 0·460(94) | 0·661(21) | 0·667(21) | 0·072(12) |
| 0·60 | 0·050(7) | 0·910(38) | 0·142(58) | 0·514(99) | 0·677(22) | 0·664(31) | 0·068(11) |
| 0·80 | 0·053(7) | 0·859(40) | 0·850(45) | 0·481(98) | 0·661(21) | 0·663(22) | 0·073(10) |
| 0·85 | 0·052(7) | 0·926(32) | 0·893(40) | 0·505(90) | 0·684(21) | 0·673(24) | 0·071(8) |
| 0·90 | 0·045(6) | 0·947(19) | 0·939(22) | 0·471(94) | 0·692(21) | 0·686(24) | 0·058(7) |
| 0·90[a] | 0·042(6) | 0·945(6) | 0·931(16) | 0·587(87) | 0·686(21) | 0·682(17) | 0·053(7) |
| 0·94 | 0·039(6) | 0·967(9) | 0·963(9) | 0·694(70) | 0·698(21) | 0·693(18) | 0·048(6) |
| 0·95 | 0·036(6) | 0·972(10) | 0·972(10) | 0·714(77) | 0·696(19) | 0·702(21) | 0·044(7) |
| 0·97 | 0·031(4) | 0·983(8) | 0·982(8) | 0·811(60) | 0·699(19) | 0·700(17) | 0·037(6) |
| 0·98 | 0·029(5) | 0·988(7) | 0·989(8) | 0·857(64) | 0·696(20) | 0·700(17) | 0·035(6) |
| 0·99 | 0·027(6) | 0·995(4) | 0·995(4) | 0·918(42) | 0·702(24) | 0·705(20) | 0·032(6) |
| 1·00 | 0·025(5) | 1·000 | 1·000 | 1·000 | 0·709(19) | 0·702(18) | 0·030(6) |
| 1·00[a] | 0·025(6) | 1·000 | 1·000 | 1·000 | 0·708(20) | 0·704(18) | 0·029(6) |
| 0·50[b] | 0·216(18) | 0·882(14) | 0·079(15) | — | 0·702(17) | 0·714(22) | — |
| 0·50[b] | 0·384(21) | 0·086(16) | 0·911(15) | — | 0·730(18) | 0·726(19) | — |
| | | | Mixture II | | | | |
| 1·00 | 0·042(6) | 1·000 | 1·000 | 1·000 | 0·611(39) | 0·612(24) | 0·074(15) |
| 0·98 | 0·040(5) | 0·978(9) | 0·978(15) | 0·997(8) | 0·623(37) | 0·621(22) | 0·069(13) |
| 0·97[c] | 0·039(6) | 0·967(2) | — | 0·995(10) | 0·629(23) | — | 0·066(16) |
| 0·50 | 0·036(5) | 0·965(23) | 0·096(19) | 0·995(10) | 0·621(33) | 0·878(10) | 0·060(10) |
| 0·07[c] | 0·011(6) | — | 0·031(19) | 0·988(71) | — | 0·884(11) | 0·022(8) |
| 0·04[c] | 0·008(7) | — | 0·022(12) | 0·980(81) | — | 0·885(10) | 0·016(14) |
| 0·02[c] | 0·004(2) | — | 0·011(5) | 0·934(98) | — | 0·882(9) | 0·005(3) |
| 0·00 | $5 \times 10^{-5}(20)$ | 0·000 | 0·000 | 0·000 | 0·884(10) | 0·882(10) | $6 \times 10^{-5}(25)$ |
| 0·50[b] | 0·061(13) | 0·945(24) | 0·084(22) | — | 0·647(8) | — | — |
| 0·50[b] | 0·149(15) | 0·938(25) | 0·088(22) | — | 0·676(10) | 0·884(14) | — |
| 0·50[b] | 0·143(14) | 0·944(24) | 0·093(98) | — | 0·669(9) | 0·882(16) | — |

[a] Simulation with a different total number of particles.
[b] Two-box simulation in the liquid–liquid (LL) two-phase region.
[c] Two-box simulation in the liquid–vapour (LV) two-phase region.

computational procedures were similar to those discussed in section 3.

A swapping of the identity of the two boxes containing two immiscible liquid phases was found in mixtures III and V, near the ends of the immiscibility windows. In such cases the composition of the phases at equilibrium was determined by accumulating the simulation results for the compositions in a histogram and selecting the maxima.

### 4.2. *Simulation results*

The interaction parameters for the ternary mixtures studied are also reported in table 1. In both mixtures all three components have identical size and self-interaction parameters, i.e., phase separation is due only to weaker cross-interactions.

The simulation data obtained for the thermodynamic properties on the coexistence curve (LLV and LLLV equilibria) of the three mixtures are presented in table 3. The internal consistency of the data was checked using criteria (i) and (iii) of section 3.

The $x$–$y$ ternary diagrams for mixtures III–V are shown in figures 5–7. The symmetry of the diagrams is a consequence of the identity between all pure-component parameters and the choice of cross-parameters representing identical interactions between all components (mixtures III and IV) or a third component exhibiting the same affinity for the other two (symmetrical amphiphilic behaviour in mixture V).

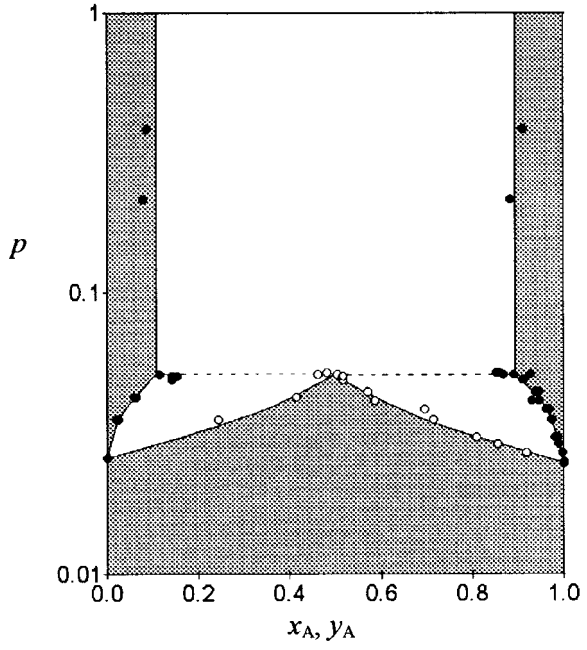


Figure 3. Phase diagram ($p$–$x$–$y$) for mixture I at $T = 1{\cdot}0$. Shaded and blank areas correspond to one-phase and two-phase regions; filled and open circles refer to simulation data in the liquid and vapour phases, respectively; and the dashed line marks the region where LLV equilibria occur.

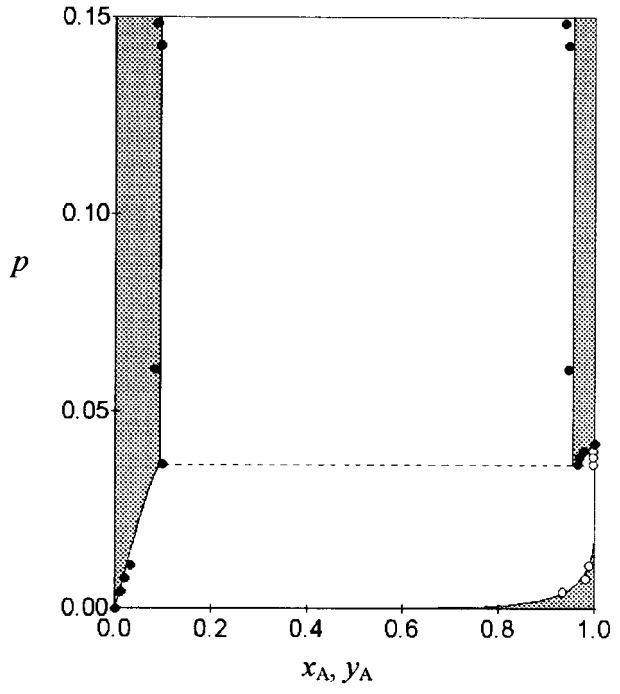


Figure 4. Phase diagram ($p$–$x$–$y$) for mixture II at $T = 0{\cdot}8$; symbols as for figure 3.

Table 3. Results for phase coexistence properties of ternary mixtures: $p$–$x$–$y$ and density data.

| $x_{A,B\,total}$[a] | $p_{vap}$ | $x_{A,B,liq.1}$ | $x_{A,B,liq.2}$ | $x_{A,B,liq.3}$ | $y_{A,B}$ | $\rho_{liq.1}$ | $\rho_{liq.2}$ | $\rho_{liq.3}$ | $\rho_{vap.}$ |
|---|---|---|---|---|---|---|---|---|---|
| | | | | Mixture III | | | | | |
| 0·500 | 0·056(8) | 0·874(53) | 0·125(45) | — | 0·51(15) | 0·667(27) | 0·668(25) | — | 0·080(17) |
| 0·500 | | 0·126(57) | 0.875(63) | — | 0·49(15) | | | | |
| 0·485 | 0·062(7) | 0·804(57) | 0·150(16) | — | 0·47(10) | 0·650(27) | 0·655(26) | — | 0·093(17) |
| 0·485 | | 0·174(58) | 0·830(60) | — | 0·45(10) | | | | |
| 0·480 | 0·063(7) | 0·790(64) | 0·154(56) | — | 0·46(11) | 0·643(28) | 0·652(27) | — | 0·097(16) |
| 0·480 | | 0·181(77) | 0·819(82) | — | 0·44(11) | | | | |
| 0·000 | 0·057(8) | 0·000 | 0·000 | — | 0·000 | 0·664(23) | 0·673(22) | — | 0·085(18) |
| 0·500 | | 0·147(52) | 0·884(64) | — | 0·51(15) | | | | |
| 0·030 | 0·058(8) | 0·023(7) | 0·025(8) | — | 0·09(4) | 0·654(23) | 0·644(23) | — | 0·078(15) |
| 0·485 | | 0·839(37) | 0·153(44) | — | 0·45(13) | | | | |
| 0·050[b] | 0·061(9) | 0·043(8) | 0·043(8) | — | 0·12(5) | 0.649(24) | 0·596(23) | — | 0·091(19) |
| 0·475[b] | | 0·269(30) | 0·688(60) | — | 0·44(12) | | | | |
| 0·070[b] | 0·068(9) | 0·060(10) | 0·060(10) | — | 0·15(5) | 0·625(23) | 0·597(31) | — | 0·110(20) |
| 0·465[b] | | 0·321(50) | 0·619(60) | — | 0·43(13) | | | | |
| 0·460[b] | 0·069(9) | 0·316(40) | 0·614(50) | — | 0·42(12) | 0·618(43) | 0·598(26) | — | 0·110(20) |
| 0·460[b] | | 0·614(50) | 0·316(40) | — | 0·42(11) | | | | |
| 0·500 | 0·054(7) | 0·130(40) | 0·891(41) | — | 0·51(12) | 0·664(24) | 0·673(22) | — | 0·076(25) |
| 0·000 | | 0·000 | 0·000 | — | 0·000 | | | | |
| 0·490 | 0·061(9) | 0·142(46) | 0·867(48) | — | 0·47(14) | 0·659(25) | 0·669(23) | — | 0·091(19) |
| 0·020 | | 0·016(7) | 0·014(7) | — | 0·06(3) | | | | |
| 0·480 | 0·059(8) | 0·813(97) | 0·189(86) | — | 0·45(14) | 0·646(29) | 0·634(29) | — | 0·084(18) |
| 0·040 | | 0·031(11) | 0·034(11) | — | 0·12(5) | | | | |
| 0·460[b] | 0·062(8) | 0·336(30) | 0·587(50) | — | 0·42(15) | 0·584(23) | 0·595(24) | — | 0·090(21) |
| 0·080[b] | | 0·078(10) | 0·078(10) | — | 0·164(5) | | | | |

(*Continued*)

Table 3. (*Continued*).

| $x_{A,B\,total}$[a] | $p_{vap}$ | $x_{A,B,liq.1}$ | $x_{A,B,liq.2}$ | $x_{A,B,liq.3}$ | $y_{A,B}$ | $\rho_{liq.1}$ | $\rho_{liq.2}$ | $\rho_{liq.3}$ | $\rho_{vap.}$ |
|---|---|---|---|---|---|---|---|---|---|
| | | | | Mixture IV | | | | | |
| 0·500 | 0·059(10) | 0·037(21) | 0·967(32) | — | 0·49(15) | 0·686(30) | 0·691(27) | — | 0·082(19) |
| 0·500 | | 0·963(56) | 0·033(20) | — | 0·51(16) | | | | |
| 0·480 | 0·069(11) | 0·038(25) | 0·951(64) | — | 0·43(15) | 0·691(34) | 0·685(34) | — | 0·096(20) |
| 0·480 | | 0·947(61) | 0·034(24) | — | 0·41(14) | | | | |
| 0·466 | 0·076(12) | 0·042(31) | 0·938(71) | — | 0·39(13) | 0·687(36) | 0·679(40) | — | 0·111(20) |
| 0·466 | | 0·993(62) | 0·038(26) | — | 0·38(12) | | | | |
| 0·333 | 0·098(18) | 0·048(30) | 0·910(71) | 0·043(16) | 0·35(10) | 0·675(43) | 0·679(50) | 0·682(48) | 0·204(28) |
| 0·333 | | 0·907(65) | 0·043(20) | 0·039(15) | 0·31(10) | | | | |
| 0·000 | 0·056(10) | 0·000 | 0·000 | — | 0·000 | 0·689(29) | 0·689(27) | — | 0·077(18) |
| 0·500 | | 0·036(20) | 0·968(51) | — | 0·49(16) | | | | |
| 0·500 | 0·055(10) | 0·040(25) | 0·967(56) | — | 0·49(15) | 0·688(29) | 0·691(27) | — | 0·086(19) |
| 0·000 | | 0·000 | 0·000 | — | 0·000 | | | | |
| 0·480 | 0·077(11) | 0·047(29) | 0·953(78) | — | 0·45(14) | 0·682(33) | 0·693(31) | — | 0·119(23) |
| 0·040 | | 0·015(12) | 0·012(10) | — | 0·13(3) | | | | |
| 0·060 | 0·078(11) | 0·022(15) | 0·019(13) | — | 0·20(3) | 0·681(29) | 0·683(30) | — | 0·116(17) |
| 0·470 | | 0·939(53) | 0·036(19) | — | 0·40(9) | | | | |
| 0·460 | 0·087(13) | 0·041(30) | 0·938(71) | — | 0·39(9) | 0·687(35) | 0·688(35) | — | 0·143(22) |
| 0·480 | | 0·026(19) | 0·025(26) | — | 0·22(3) | | | | |
| 0·100 | 0·092(13) | 0·030(20) | 0·028(11) | — | 0·26(3) | 0·686(34) | 0·688(35) | — | 0·157(21) |
| 0·450 | | 0·927(81) | 0·038(27) | — | 0·37(9) | | | | |
| | | | | Mixture V | | | | | |
| 0·500 | 0·059(8) | 0·037(16) | 0·967(55) | — | 0·49(16) | 0·686(13) | 0·691(22) | — | 0·082(17) |
| 0·500 | | 0·963(47) | 0·033(17) | — | 0·51(14) | | | | |
| 0·465 | 0·050(7) | 0·046(18) | 0·893(34) | — | 0·49(13) | 0·689(23) | 0·687(22) | — | 0·065(12) |
| 0·465 | | 0·882(40) | 0·039(19) | — | 0·47(12) | | | | |
| 0·430 | 0·048(7) | 0·056(24) | 0·799(41) | — | 0·46(14) | 0·684(22) | 0·681(24) | — | 0·063(14) |
| 0·430 | | 0·805(37) | 0·061(25) | — | 0·46(13) | | | | |
| 0·400 | 0·048(7) | 0·078(38) | 0·679(52) | — | 0·44(14) | 0·681(24) | 0·670(26) | — | 0·064(14) |
| 0·400 | | 0·719(72) | 0·104(59) | — | 0·45(13) | | | | |
| 0·365 | 0·045(7) | 0·120(45) | 0·602(49) | — | 0·42(13) | 0·673(25) | 0·672(25) | — | 0·060(13) |
| 0·365 | | 0·601(57) | 0·119(48) | — | 0·42(13) | | | | |
| 0·335[b] | 0·041(6) | 0·273(50) | 0·369(50) | — | 0·40(12) | 0·663(21) | 0·667(27) | — | 0·052(11) |
| 0·335[b] | | 0·384(50) | 0·282(50) | — | 0·41(12) | | | | |
| 0·300 | 0·037(6) | 0·291(49) | 0·298(51) | — | 0·38(12) | 0·661(32) | 0·665(21) | — | 0·046(10) |
| 0·300 | | 0·294(53) | 0·292(49) | — | 0·39(13) | | | | |

[a] The subscripts A and B refer to the first and second component's mole fractions, respectively. These are shown in two successive rows in the table.

[b] Due to identity interchange of the two boxes containing the liquid phases, the results presented were obtained by arranging the simulation data in a concentration histogram and selecting the concentrations corresponding to the maxima of the plot.

The components of mixture III have the same interaction parameters as those in mixture I (cf. table 1). The three sides of the ternary diagram shown in figure 5 (binary mixtures A + B, A + C and B + C) correspond to the three-phase line in mixture I (cf. figure 3). When a small amount of the third component is added to these binary mixtures its concentration is not large enough to form a new liquid phase rich in that component. This means that the added component will have to distribute itself between the already existing liquid and vapour phases. The interactions in those phases will become weaker, pressure will increase and the immiscibility window will become narrower. In the case of mixture III the immiscibility windows close before the added component reaches a concentration suitable for the formation of a third liquid phase: the phase diagram shows three immiscibility windows (LLV equilibria) adjacent to the sides of the ternary diagram.

If the interactions between components are decreased, the three immiscibility LI windows of figure 5 will expand and will eventually overlap. This situation was analysed in mixture IV, where all cross-interaction parameters were reduced from 0·7 to 0·6. Weak interactions between all three components produces a diagram showings almost complete immiscibility between them (figure 6). The diagram also shows a four-phase (triple immiscibility) line: if all components are present in the mixture with a concentration larger than about

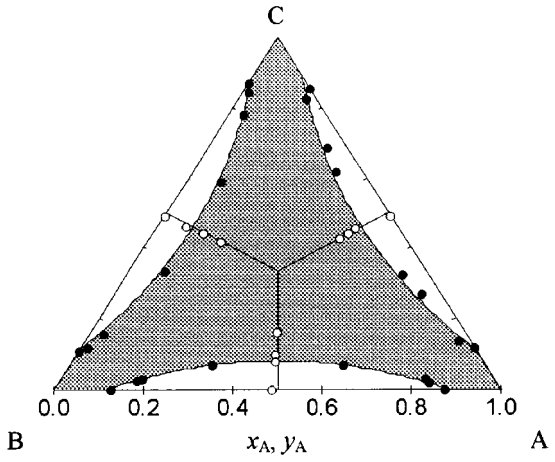


Figure 5. Phase diagram ($x$–$y$) for mixture III at $T$ = 1·0 and $p$ = orthobaric pressure. Shaded and blank areas correspond to two-phase and three-phase regions; and filled and open circles refer to simulation data in the liquid and vapours phases, respectively.

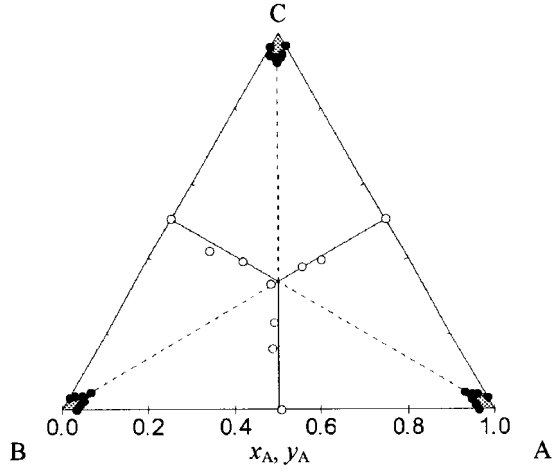


Figure 6. Phase diagram ($x$–$y$) for mixture IV at $T$ = 1·0 and $p$ = orthobaric pressure; symbols as for figure 5; and the dashed lines mark the region exhibiting triple immiscibility (LLLV equilibria).

5% three liquid phases, each rich in one of the components, will be at equilibrium with an equimolar vapour phase (the four points joined by the dashed line in figure 6). A mixture of type I (alkane + perfluoroalkane) mixed with a strongly polar species may exhibit such behaviour.

In the case of mixture V the $\varepsilon_{AB}$ interaction was kept at 0·6 but the cross-interaction parameters between component C and the other two components were increased to unity (amphiphilic behaviour of the third component). Figure 7 shows a diagram exhibiting a

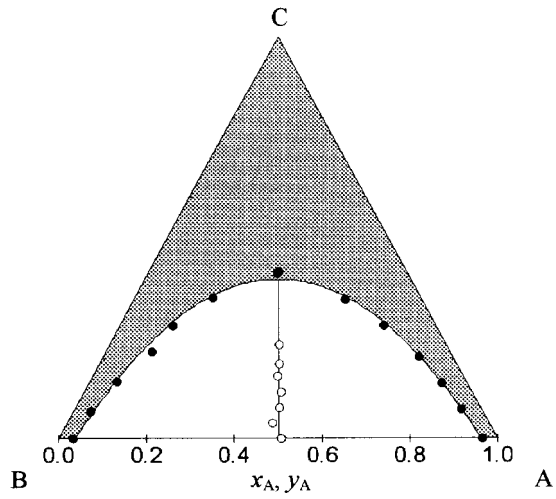


Figure 7. Phase diagram ($x$–$y$) for mixture V at $T$ = 1·0 and $p$ = orthobaric pressure; symbols as for figure 5: and data points shown in the diagram except the one with 0·300 total mole fraction in A and B (cf. table 3) correspond to regions exhibiting LLV equilibria.

large immiscibility window between A and B that decreases when C is added to the system. Considering again an (alkane + perfluoroalkane) system, a third component could be in this case a suitably partially fluorinated alkane.

## 5. Conclusion

The Gibbs simulation method can be extended to study multiphase equilibria by increasing the number of boxes. The boxes are considered in pairs so that the rules for the particle and volume exchanges and the methods for dealing with mixtures and long range corrections can be carried over directly from the two-phase simulations.

Whenever the number of phases is smaller than the number of boxes then at least two of the boxes will be at the same density. We have to exercise considerable care in this case since one box may reduce both $N$ and $V$ simultaneously, leading to problems as the box length becomes smaller than a sensible cut-off in the potential and the box eventually disappears. We recommend checking the results by reducing the number of boxes in this case. On the positive side, it is much easier to equilibrate two dense fluids when they are in equilibrium with their vapour, since the rate of acceptance for particle exchange moves between liquid and vapour is much higher than that between two liquids.

We have demonstrated that the method works well by simulating model systems exhibiting three- and four-phase equilibria. The equality of the pressure and chemical potential in the coexisting phases and the

symmetry of the phase diagrams indicates that the method can be applied reliably to these systems. As an additional check for two-component systems in a two-phase region we note that the same results are obtained using the many-box and the two-box algorithms.

We have been able to simulate three- and four-phase equilibria successfully for atomic systems, and the ideas can be extended readily to molecular fluids and to the simulation of chain molecules by applying configurational bias sampling methods.

J.N.C.L. acknowledges the support from the Gulbenkian Foundation (Programa Gulbenkian de Estímulo à Investigação/95) and the Junta Nacional de Investigação Cientifica e Tecnológica (PRAXIS XXI/BPD/6036/95 and PBIC/C/QUI/2195/95). D.J.T. wishes to thank the EPSRC for grant GR/K 83878 for computing equipment.

## References

[1] Panagiotopoulos, A. Z., 1987, *Molec. Phys.*, **61,** 813.
[2] Panagiotopoulos, A. Z., 1992, *Molec. Simulation*, **9,** 1.
[3] Smit, B., 1992, *Computer Simulation in Chemical Physics*, Nato ASI Series, series C, vol. 137, edited by M. P. Allen and D. J. Tildesley (Dordrecht: Kluwer).
[4] Panagiotopoulos, A. Z., Quirke, N., Stapleton, M., and Tildesley, D. J., 1988, *Molec. Phys.*, **63,** 527.
[5] Ruli, L. F., Jackson, G., and Smit, B., 1995, *Molec. Phys.*, **85,** 435.
[6] van Leeuwen, M. E., Peters, C. J., de Swaan Arons, J., and Panagiotopoulos, A. Z., 1991, *Fluid Phase Equilibria*, **66,** 57.
[7] Adams, D. J., 1976, *Molec. Phys.*, **32,** 647.
[8] Rowlinson, J. S., and Swinton, F. L., 1982, *Liquids and Liquid Mixtures,* 3rd Edn (London: Butterworths).